Zhu et al. *Zool. Res.* 2024, 45(1): 79−94
https://doi.org/10.24272/j.issn.2095-8137.2023.022

ZR | Zoological Research

Article Open Access

Loss of *LBP* triggers lipid metabolic disorder through H3K27 acetylation-mediated C/EBPβ-*SCD* activation in non-alcoholic fatty liver disease

Ya-Ling Zhu[1,2,#], Lei-Lei Meng[1,#], Jin-Hu Ma[1,#], Xin Yuan[1], Shu-Wen Chen[1], Xin-Rui Yi[1], Xin-Yu Li[1], Yi Wang[1], Yun-Shu Tang[1,2], Min Xue[1], Mei-Zi Zhu[1], Jin Peng[1], Xue-Jin Lu[1], Jian-Zhen Huang[4], Zi-Chen Song[1], Chong Wu[1], Ke-Zhong Zheng[3], Qing-Qing Dai[3], Fan Huang[3,*], Hao-Shu Fang[1,2,*]

[1] *Department of Pathophysiology*, *Anhui Medical University*, *Hefei*, *Anhui* 230032, *China*
[2] *Laboratory Animal Research Center*, *School of Basic Medical Sciences*, *Anhui Medical University*, *Hefei*, *Anhui* 230032, *China*
[3] *Department of Hepatobiliary Surgery*, *First Affiliated Hospital of Anhui Medical University*, *Hefei*, *Anhui* 230022, *China*
[4] *College of Animal Science and Technology*, *Jiangxi Agricultural University*, *Nanchang*, *Jiangxi* 330045, *China*

ABSTRACT

Non-alcoholic fatty liver disease (NAFLD) is associated with mutations in lipopolysaccharide-binding protein (*LBP*), but the underlying epigenetic mechanisms remain understudied. Herein, *LBP*$^{-/-}$ rats with NAFLD were established and used to conduct integrative targeting-active enhancer histone H3 lysine 27 acetylation (H3K27ac) chromatin immunoprecipitation coupled with high-throughput and transcriptomic sequencing analysis to explore the potential epigenetic pathomechanisms of active enhancers of NAFLD exacerbation upon *LBP* deficiency. Notably, *LBP*$^{-/-}$ reduced the inflammatory response but markedly aggravated high-fat diet (HFD)-induced NAFLD in rats, with pronounced alterations in the histone acetylome and regulatory transcriptome. In total, 1 128 differential enhancer-target genes significantly enriched in cholesterol and fatty acid metabolism were identified between wild-type (WT) and *LBP*$^{-/-}$ NAFLD rats. Based on integrative analysis, CCAAT/enhancer-binding protein β (C/EBPβ) was identified as a pivotal transcription factor (TF) and contributor to dysregulated histone acetylome H3K27ac, and the lipid metabolism gene *SCD* was identified as a downstream effector exacerbating NAFLD. This study not only broadens our understanding of the essential role of *LBP* in the pathogenesis of NAFLD from an epigenetics perspective but also identifies key TF C/EBPβ and functional gene *SCD* as potential regulators and therapeutic targets.

Keywords: Non-alcoholic fatty liver disease; C/EBPβ; Lipopolysaccharide-binding protein; H3K27ac; Integrative analysis; Enhancer

INTRODUCTION

Non-alcoholic fatty liver disease (NAFLD), characterized by ectopic lipid accumulation in the liver, is the most prevalent chronic liver disease worldwide, affecting almost 25% of the global population (Friedman et al., 2018; Samuel & Shulman, 2018; Younossi et al., 2019). Etiologically, NAFLD demonstrates a close correlation with systemic metabolic disorders, such as obesity, insulin resistance, dyslipidemia, and hyperglycemia (Yu et al., 2019), in addition to certain genetic polymorphisms. Notably, several gene single-nucleotide polymorphisms, including Semaphorin 7A (*SEMA7A*) (Zhao et al., 2022a) and Abhydrolase domain containing 5 (*ABHD5*) (Youssefian et al., 2019), have been reported to increase susceptibility to lipid metabolic disorders in human NAFLD.

Lipopolysaccharide-binding protein (*LBP*), which is primarily produced in the hepatocytes (Zhou et al., 2016), plays a pivotal role in the inflammatory response (Pfalzgraff & Weindl, 2019; Song et al., 2021). Emerging evidence has also shown that *LBP* regulates adipogenesis, affecting hepatic lipid metabolism, and is highly associated with various metabolic

Received: 21 May 2023; Accepted: 24 August 2023; Online: 25 August 2023

Foundation items: This study was supported by the National Natural Science Foundation of China (81971875, 82300661), Natural Science Foundation of Anhui province (2308085QH246), Natural Science Foundation of the Anhui Higher Education Institutions (KJ2021A0205), Basic and Clinical Cooperative Research Program of Anhui Medical University (2019xkjT002, 2019xkjT022, 2022xkjT013), Talent Training Program, School of Basic Medical Sciences, Anhui Medical University (2022YPJH102), and National College Students Innovation and Entrepreneurship Training Program of China (202210366024)

#Authors contributed equally to this work

*Corresponding authors, E-mail: huang_f@vip.126.com; fanghaoshu@ahmu.edu.cn

disorders, including obesity (Moreno-Navarrete et al., 2015; Sun et al., 2010). Of note, patients harboring *LBP* mutations also exhibit high susceptibility to metabolic disorders (Meng et al., 2021; Takeuchi et al., 2007), raising the question of the mechanisms by which *LBP* influences the metabolic dysregulation observed in NAFLD, especially in the context of epigenetic processes.

Various studies have explored the epigenetic mechanisms related to the etiology and pathogenesis of disease (Feinberg, 2007; Ospelt, 2022). As a primary type of epigenetic modification and post-translational modification, histone H3 lysine 27 acetylation (H3K27ac) is widely recognized as a marker of active enhancers and a contributor to NAFLD pathogenesis (Rada-Iglesias et al., 2011; Smith & Shilatifard, 2014; Zhao et al., 2018; Zhu et al., 2021). For instance, Becares et al. (2019) demonstrated that liver X receptor alpha can alter H3K27ac and affect NAFLD development. Liu et al. (2018) revealed that Snail1 can mediate the deacetylation of H3K27 and prevent NAFLD. Hu et al. (2022) found that H3K27ac can activate long non-coding RNA (lncRNA) *NEAT1* and promote hepatic lipid accumulation in NAFLD. However, despite considerable efforts, the epigenetic mechanisms involved in the pathogenesis of NAFLD under *LBP* deficiency are poorly defined.

In this study, we explored the epigenomic H3K27ac and transcriptomic alterations induced by *LBP* deficiency in an experimental NAFLD model, resulting in outcomes analogous to those observed in clinical NAFLD cases with *LBP* mutation. We employed integrative epigenome H3K27ac chromatin immunoprecipitation coupled with high-throughput sequencing (ChIP-Seq) and transcriptome high-throughput RNA sequencing (RNA-Seq). Results revealed widespread NAFLD-associated histone acetylome and transcriptome changes and further identified a core transcription factor (TF) involved in the regulation and exacerbation of lipid metabolic disorder progression in NAFLD rats with *LBP* deletion. Overall, our study provided genome-wide profiling of histone acetylome and transcriptome signals underlying NAFLD pathogenesis and elucidated the role of *LBP* deficiency in accelerating NAFLD from an epigenetic perspective. These findings provide novel insights and strategies for the potential prevention and treatment of NAFLD in patients harboring *LBP* loss-of-function.

MATERIALS AND METHODS

Ethics statement

All applicable international, national, and/or institutional guidelines for the care and use of animals were strictly followed. All animal collection protocols complied with the current laws of China. All animal protocols were approved by the Ethics Committee of Anhui Medical University (Approval No. SYXK 2017-006).

Animals and treatment

$LBP^{+/+}$ (wild-type (WT)) and $LBP^{-/-}$ rats and $LBP^{+/+}$ (WT) and $LBP^{-/-}$ mice were generated at the Nanjing Biomedical Research Institute of Nanjing University, as described previously (Song et al., 2021). Male WT (n=12) and $LBP^{-/-}$ (n=12) rats aged 6 weeks and male WT (n=12) and $LBP^{-/-}$ (n=12) mice aged 8 weeks were used in this study. Animals were housed under specific pathogen-free (SPF) conditions under a 12-h light/12-h dark cycle at a temperature of 24±2 °C and humidity of 50%±10%. The NAFLD models were established by inducing rats and mice with a high-fat diet (HFD; 20.2% protein, 45.4% fat, and 34.5% carbohydrates) (XTHF45-1, Xietong Pharma, China) for 8 and 24 weeks, respectively. Rats and mice fed a normal diet (ND; 20.6% protein, 12% fat, and 67.4% carbohydrates) (SWS9102, Xietong Pharma, China) were used as controls. The animals were randomly divided into four groups: WT_ND, $LBP^{-/-}$_ND, WT_HFD, and $LBP^{-/-}$ _HFD groups. At the end of the experiments, body and liver weights were determined and serum levels of lipids, including triglycerides (TG) and total cholesterol (TC), and alanine amino transferase (ALT) and aspartate amino transferase (AST) were measured using a Hitachi 3100 Automatic Analyzer (Japan) according to the manufacturer's protocols.

Histological analysis and staining

All histological analyses were performed by Servicebio Technology (China). Briefly, fresh liver tissues were dissected and fixed in 10% neutral buffered formation, with paraffin sections then stained with a Hematoxylin and Eosin (H&E) Staining Kit (Beyotime, China). The histological samples were observed and imaged using a light microscope (ECLIPSE 80i, Nikon, Japan). To calculate the NAFLD activity score (NAS), H&E images were analyzed according to previously described criteria (Brunt et al., 2011). NAS is defined as the sum of the scores of three components: steatosis (0–3), lobular inflammation (0–3), and hepatocyte ballooning (0–2).

Reverse transcription-quantitative real-time polymerase chain reaction (RT-qPCR)

To validate mRNA expression levels, total RNA was extracted using Trizol reagent (Invitrogen, USA) and reverse-transcribed into cDNA using a Reverse Transcription Kit (Vazyme Biotech, China). A SYBR Green Premix Kit (Vazyme Biotech, China) was then used for RT-qPCR amplification, pre-denaturing cDNA at 95 °C for 10 min, followed by 40 cycles at 95 °C and 60 °C for 1 min. The relative mRNA expression levels of the target genes were normalized to *β-actin* expression using the $2^{-\Delta\Delta Ct}$ method. The primers used for RT-qPCR analysis are listed in Supplementary Table S1.

Cell culture and cell model of lipid accumulation

The hepatocyte cell line BRL-3A was purchased from the Type Culture Collection of the Chinese Academy of Sciences (Beijing, China). Cells were cultured in Dulbecco's Modified Eagle Medium (DMEM) with 10% fetal bovine serum (FBS) and placed in a humidified atmosphere with 5% CO_2 at 37 °C. After corresponding pretreatment and transfection with indicated plasmids, 0.5 mmol/L palmitic acid (PA) or 0.2 mmol/L oleic acid (OA) was added to the medium to establish an *in vitro* model of lipid accumulation in BRL-3A hepatocytes. For intracellular lipid accumulation examination, cells were fixed with 4% paraformaldehyde for 20 min and stained with 60% Oil Red O (ORO) (O1391; Sigma-Aldrich, USA) working solution.

Exploration of tissue and cellular localization of *LBP*

To explore the tissue localization of *LBP* in humans, mice, and rats, *LBP* expression in different tissues of these species was analyzed using the PRJEB4337, PRJNA66167, and PRJNA238328 datasets, respectively, from the NCBI public database (http://www.ncbi.nlm.nih.gov). The localization of *LBP* in different cell types was obtained from the Single Cell

Type database in the Human Protein Atlas (https://www.proteinatlas.org/).

High-throughput RNA sequencing (RNA-Seq) and differential gene expression analysis

RNA was isolated from the liver tissues of WT and *LBP*$^{-/-}$ rats fed with ND or HFD separately using a Trizol Kit (Invitrogen, USA) according to the manufacturer's protocols. The extracted samples were then used for library construction, and 150 bp paired-end sequencing was performed using the HiSeq 4000 platform (Illumina, USA).

Sequenced reads were mapped to the rat reference genome *Rattus_norvegicus*_6.0 by STAR-2.5.3a (Dobin et al., 2013). Read quality was assessed using the FastQC tool (http://www.bioinformatics.babraham.ac.uk/projects/fastqc). Low-quality and adapter sequences were trimmed using Trimmomatic. Afterwards, the expression of transcripts was quantified using the Salmon tool (Sewe et al., 2022), and estimates of transcript abundance for gene-level analysis were imported and summarized using the tximport (Soneson et al., 2015) function in the R/Bioconductor software suite. Finally, DESeq2 (Love et al., 2014) was employed to identify differentially expressed genes (DEGs) between WT and *LBP*$^{-/-}$ rats based on the criteria $|\log_2$ (fold-change)$|\geq 1.5$ and $P<0.05$.

Chromatin immunoprecipitation with high-throughput sequencing (ChIP-Seq) and differential analysis of histone acetylome signals

Chromatin immunoprecipitation assay was performed using a SimpleChIP Enzymatic Chromatin IP Kit (9005, Cell Signaling Technology, USA). Firstly, 150 mg of liver tissue was crosslinked with 1% formaldehyde, with the process then terminated with ice-cold phosphate-buffered saline (PBS) containing 0.125 mol/L glycine and protease inhibitor. The samples were lysed by the addition of lysis buffer and disrupted with a homogenizer, followed by the sheared of chromatin to an average size of 100–500 bp using sonication and micrococcal nuclease. The sheared chromatin was then immunoprecipitated with 500 μg of chromatin and 5 μg of anti-H3K27ac antibody (39133, Active Motif, China). Histone H3 (4620, Cell Signaling Technology, USA) and immunoglobulin G (IgG) (2729, Cell Signaling Technology, USA) were used as positive and negative controls, respectively. DNA fragments were collected and purified using protease and RNAase, and qPCR was also conducted using 1% input DNA to confirm ChIP success. Input library construction and sequencing procedures were carried out according to the Illumina protocols with minor modifications (Illumina, USA).

Sequencing reads were aligned to the rat reference genome *Rattus_norvegicus*_6.0 using a Burrows-Wheeler Aligner (BWA) (Abuín et al., 2015). The peak caller of Model-based Analysis for ChIP-Seq v.2.1.0 (MACS 2.1.0) was then used to identify the region enriched by H3K27ac, setting the *Q*-value threshold to 1e-5 (Zhang et al., 2008). The output peak files then were sorted and merged to skip short segments with small gaps using bedtools v.2.27.0 (Quinlan & Hall, 2010), merging those with more than 1 kb distance (merged regions were considered putative active enhancers if the region boundaries were ≥1 kb from the transcript start site (TSS)), following previous study (Villar et al., 2015). Subsequently, the SAMtools (v.1.2) "bedcov" function (Li et al., 2009) was adopted to quantify acetylated peak coverage for peak read depth according to the read counts of BAM files. ChIP and input read counts were normalized by peak lengths, subtracting input coverage from ChIP coverage to reduce the impact of fragmentation bias.

Differentially acetylated peaks between WT and *LBP*$^{-/-}$ individuals were identified using the DESeq2 R package (Love et al., 2014) in R v.3.5.1, with threshold criteria of $P<0.05$ and $|\log_2$(fold-change)$|\geq 1$. Super-enhancers were identified using the ROSE algorithm following previous reported methods (Whyte et al., 2013), defined as groups of putative enhancers in close genomic proximity (12.5 kb) with signal densities higher than the threshold (plot slope>1).

Gene Ontology (GO) and pathway enrichment analysis

DAVID (http://david-d.ncifcrf.gov/) and Metascape (https://metascape.org/gp/) were used to interpret the over-represented terms and biological processes of DEGs and differentially expressed peak-genes. The significance threshold criteria were set to $P<0.05$ and false discovery rate (FDR)≤0.05.

Integrative analysis of H3K27ac ChIP-Seq and RNA-Seq

To identify putative H3K27ac peak target genes, acetylome H3K27ac ChIP-Seq and transcriptome RNA-Seq integrative analyses were conducted by calculating the correlation between each H3K27ac peak and gene transcriptional level (Takahashi et al., 2015). Selection criteria for peak-gene correlation were defined by Pearson correlation coefficient≥0.8 and $P<0.01$. Genome-wide "four-way" analysis was performed based on the regulatory direction of differential peak-genes influenced by H3K27ac, with threshold criteria set to |Cor (peak-gene correlation)|≥0.5 and $|\log_2$(fold-change)$|\geq 1.5$, to screen PP peak-genes (up-regulated peak-genes positively regulated by H3K27ac ($\log_2$(fold-change) (ChIP≥0 & RNA≥0))) for further investigation.

Determination of core TFs

To screen core TFs in the *LBP* deficiency model, the PP peak-genes were first compared with the public Human ENCODE database (http://genome.ucsc.edu/ENCODE), then classified into 15 overlapping PP peak-genes in the livers of *LBP*$^{-/-}$ rats fed with ND and HFD. The sequences of the overlapping PP peak-genes were separately submitted to PROMO (http://alggen.lsi.upc.es/) for the identification of putative TFs. Subsequently, to investigate the interaction of putative TFs and identify core TFs, the Search Tool for the Retrieval of Interacting Genes (STRING) v,11.5 database (http://string-db.org/) was used to construct a protein-protein interaction (PPI) (Szklarczyk et al., 2017) network of predicted TFs. Combined scores of interactions higher than 0.4 were considered as significant. Metascape (https://metascape.org/gp/) was employed to examine the biological processes potentially regulated by these PP peak-genes.

To further confirm core TFs, gene homology analysis was conducted using UniProt (http://www.uniprot.org/) to determine TF conservation among humans, rats, and mice. The *LBP* promoter sequences of humans, rats, and mice were obtained from the UCSC Genome Browser (https://genome-store.ucsc.edu/) and *LBP* enhancer sequences were detected using our H3K27ac ChIP-Seq data. The sequences were then separately submitted to PROMO (http://alggen.lsi.upc.es/) to verify the core TF CCAAT/enhancer-binding protein β (C/EBPβ).

To determine the binding sites of C/EBPβ with the target gene stearoyl-CoA desaturase (*SCD*), the promoter sequence of *SCD* was obtained from the UCSC Genome Browser

(https://genome-store.ucsc.edu/) and binding site prediction was conducted using the JASPAR database (http://jaspar.genereg.net/).

Western blot analysis

Fresh liver tissues were washed with PBS and lysed in Radio Immunoprecipitation Assay (RIPA) protein lysis buffer. Insoluble material was then removed by centrifugation at 12 000 ×*g* for 20 min at 4 °C, with the resulting supernatant collected and stored at −80 °C until further use. Total protein was extracted and quantified using a BCA Protein Assay Kit (Beyotime, China). The proteins were then separated by 10%, 12%, or 15% sodium dodecyl-sulfate polyacrylamide gel electrophoresis (SDS-PAGE) and transferred to polyvinylidene fluoride (PVDF) membranes (ISEQ00010; Millipore, USA). The blotted membranes were blocked with 5% skim milk in Tris-buffered saline with Tween® 20 (TBST), then incubated with primary antibodies against H3K27ac (39133, Active motif, China, 1:1 000 dilution), C/EBPβ (23431-1-AP, Proteintech, China, 1:800 dilution), SCD (28678-1-AP, Proteintech, China, 1:10 000 dilution), LBP (23559-1-AP, Proteintech, 1:1 000 dilution), β-actin (66009-1-Ig, Proteintech, China, 1:50 000 dilution) at 4 °C overnight, then finally coated with appropriate horseradish peroxidase (HRP)-conjugated secondary antibodies (Proteintech, China, 1:10 000 dilution). Protein expression was detected using the Tanon 5200 Series Fully Automated Chemiluminescence/Fluorescence Image Analysis System (Tanon, China).

Plasmid constructs and SCD inhibition

For *LBP* and *SCD* knockdown in BRL-3A hepatocytes, small interfering RNA (siRNA) targeting *LBP* or *SCD* was designed by Shanghai GenePharma (China). For SCD inhibition, the SCD inhibitor A939572 was purchased from MedChemExpress (China). For *C/EBPβ* overexpression in the BRL-3A cells, the *C/EBPβ* overexpression plasmid (pcDNA3.1-*C/EBPβ*) was purchased from Shanghai GenePharma (China). Cells were transfected using Lipofectamine® 2000 transfection reagent (Invitrogen, USA) according to the manufacturer's protocols. Cells were harvested 48 h after transfection for further experiments.

Luciferase reporter assay

To confirm the regulatory role of C/EBPβ in *SCD* expression, sequences of three predicted C/EBPβ-binding sites in the *SCD* promoter region were cloned into the pGL3-promoter vector (containing an SV-40 promoter upstream of the luciferase gene) (Promega, USA). *C/EBPβ* was also cloned into the pCDNA 3.1 vector. For the luciferase assay, BRL-3A cells were cultured in six-well tissue culture dishes to 60% confluency by the time of transfection. Plasmids containing C/EBPβ-binding sites in the *SCD* promoter region were co-transfected with a plasmid carrying C/EBPβ using Lipofectamine® 2000 reagent (Invitrogen, USA). Six hours after transfection, the medium was changed to HDMEM supplemented with 10% FBS before overnight culture at 37 °C. To test luciferase activity, cells were collected and assessed using a Dual-Luciferase Reporter Assay Kit (Promega, USA). All primer information for plasmids is shown in Supplementary Table S2.

DNA pull-down assay

Biotin- and non-biotin-labeled DNA fragments of the *SCD* promoter were amplified by PCR. BRL-3A cells were first lysed, after which nucleoprotein was extracted and quantified using standard procedures. The desired biotin- or non-biotin-labeled DNA was added to nucleoprotein supernatant and placed in tubes on a rocker and incubated at 4 °C for 1 h. Then, 40 μL of streptavidin-conjugated agarose was added to each tube, which were again placed on the rocker for 30 min to allow affinity binding of streptavidin with biotin. The collected streptavidin-conjugated agarose beads were added with 500 μL of lysis buffer five times, followed by the addition of 40 μL of 2×SDS sample buffer to each sample for western blot analysis.

Statistical analysis

All data are presented as mean±standard deviation (SD) and were analyzed using GraphPad Prism v.9.0 (GraphPad Software, USA). Differences between groups were analyzed using Student's *t*- test or one-way analysis of variance (ANOVA) as appropriate. Here, $P < 0.05$ was considered statistically significant.

RESULTS

LBP knockout attenuates inflammatory response but aggravates HFD-induced NAFLD in rats

To elucidate the role of *LBP* in NAFLD pathogenesis, rat and mouse strains with *LBP* deletions (*LBP*$^{-/-}$), mimicking clinical cases of *LBP* mutations, were constructed. Deletion efficiency was validated by agarose gel electrophoresis and western blot (Supplementary Figure S1A, B). Both WT and *LBP*$^{-/-}$ rats were fed ND and HFD for 8 weeks (Figure 1A). Notably, minimal differences were observed between the *LBP*$^{-/-}$_ND rats and WT_ND controls (Figure 1B–K). Examination of the morphology, H&E staining, and immunostaining of livers from *LBP*$^{-/-}$_HFD rats revealed reduced inflammation but increased lipid deposition relative to the WT_HFD rats (Figure 1B, C; Supplementary Figure S2A, B). Consistently, decreased mRNA expression of proinflammatory cytokines (Tumor necrosis factor-α (TNF-α) and Interleukin-6 (IL6)) was also observed, with more severe hypertriglyceridemia and hypercholesterolemia (TG and TC) in *LBP*$^{-/-}$ _HFD rats compared to WT_HFD rats (Figure 1D–G). In addition, although *LBP* knockout reduced the body weight of HFD-fed rats, the *LBP*$^{-/-}$_HFD rats showed increased liver damage and NAFLD progression, as evidenced by higher serum transaminase (e.g., ALT and AST) levels, liver indices, and NAS values compared to the HFD-fed controls (Supplementary Figure S2C, D; Figure 1H, K). Together, these results suggest that *LBP* knockout may reduce the inflammatory response but aggravate HFD-induced NAFLD in rats.

Hepatocyte-specific _LBP_ ablation deteriorates lipid accumulation _in vitro_

To further confirm the biological consequences of *LBP* depletion, the tissue-specific expression and cellular localization of *LBP* were first determined. Results showed that *LBP* expression in the liver far exceeded that in other tissues across humans, rats, and mice (Figure 2A–C). Among the different liver cells, hepatocytes exhibited predominant *LBP* cellular localization, as evidenced by RNA single-cell type specificity analysis (Figure 2D, E). *LBP*- knockdown BRL-3A hepatocytes were then constructed through transduction using siRNA targeting the *LBP* gene *in vitro*, which was confirmed by western blot and RT-qPCR (Supplementary Figure 1C, D). Consistent with the *in vivo* NAFLD model, *LBP*-ablated

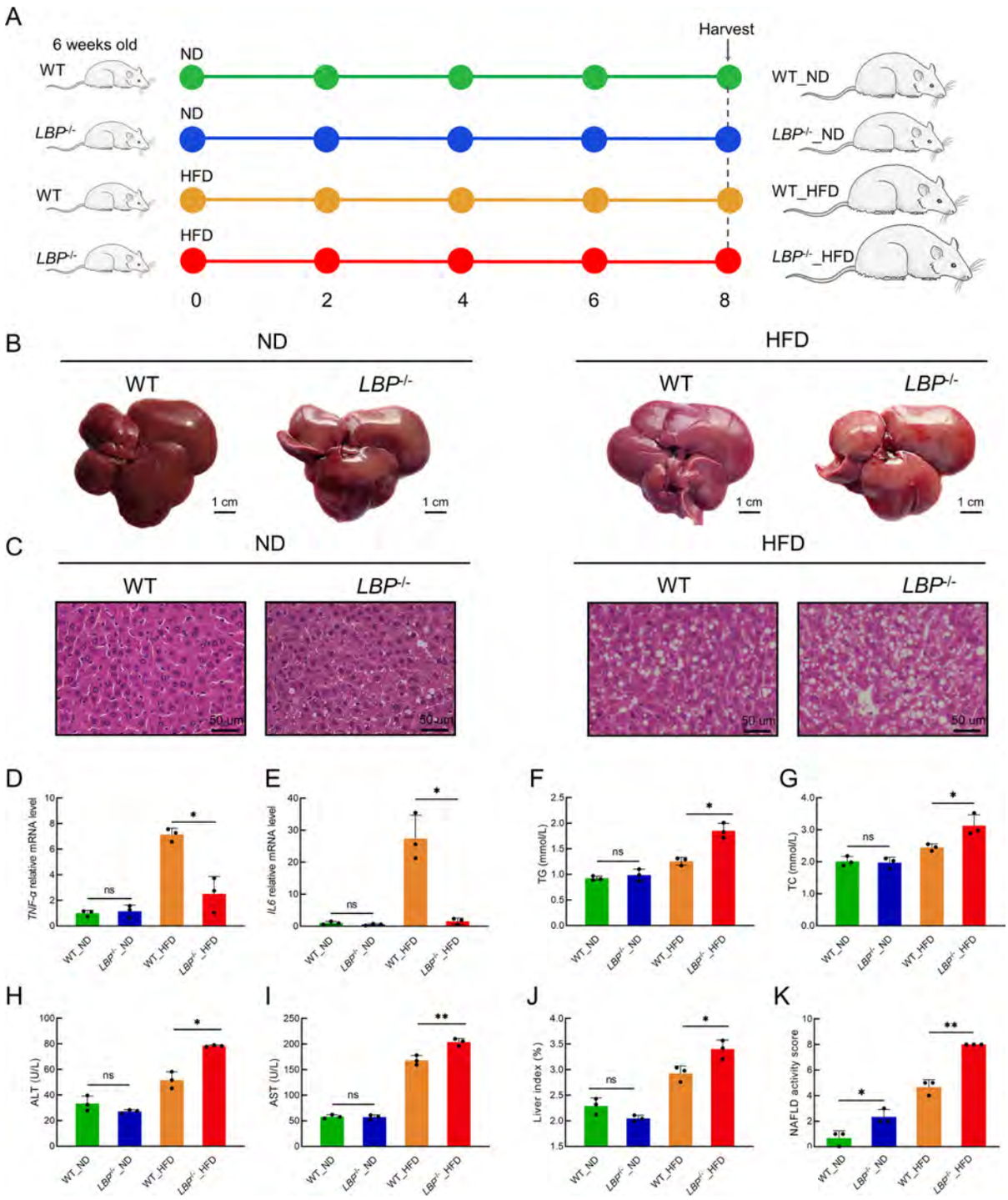

Figure 1 *LBP* knockout reduces inflammatory response but exacerbates HFD-induced NAFLD process in rats

A: Schematic showing groupings and steps of animal experiments. WT and *LBP*$^{-/-}$ rats were fed with ND or HFD for 8 weeks (*n*=6/group). B, C: Representative morphology (B) (scale bar: 1 cm) and H&E staining (C) (scale bar: 50 μm) of liver sections from WT_ND, *LBP*$^{-/-}$_ND, WT_HFD, and *LBP*$^{-/-}$_HFD rats (*n*=6/group). D, E: Relative mRNA expression levels of *TNF-α* (D) and *IL6* (E) in liver of WT_ND, *LBP*$^{-/-}$_ND, WT_HFD, and *LBP*$^{-/-}$_HFD rats (*n*=3/group). F–I: Serum content of TG (F), TC (G), ALT (H), and AST (I) in indicated groups (*n*=3/group). J: Liver index in indicated groups (*n*=3/group). K: Quantification of NAS in indicated groups *(n*=3/group). NAS is defined as the sum of scores of three components: steatosis (0–3), lobular inflammation (0–3), and hepatocyte ballooning (0–2). One-way ANOVA of data was performed. ns: Not significant; *: *P<0.05*; **: *P*<0.01. All data are shown as mean±SD. ND: Normal diet, HFD: High-fat diet, *TNF-α*: Tumor necrosis factor-α, *IL6*: Interleukin 6, TG: triglyceride, TC: total cholesterol, ALT: alanine transaminase, AST: aspartate transaminase, Liver index: liver weight to body weight ratio, NAFLD: non-alcoholic fatty liver disease, NAS: NAFLD activity score.

hepatocytes exhibited no significant differences compared to their controls under bovine serum albumin (BSA) treatment (Figure 2F, G). However, hepatocyte-specific ablation of *LBP* markedly decreased the expression of inflammation-related genes (*TNF-α*, *IL6*) (Figure 2F) and markedly increased the expression of lipid storage-related genes (*FASN*, *SREBP1*c) under PA treatment (Figure 2G). Together, these results indicate that hepatocyte-specific ablation of *LBP* may

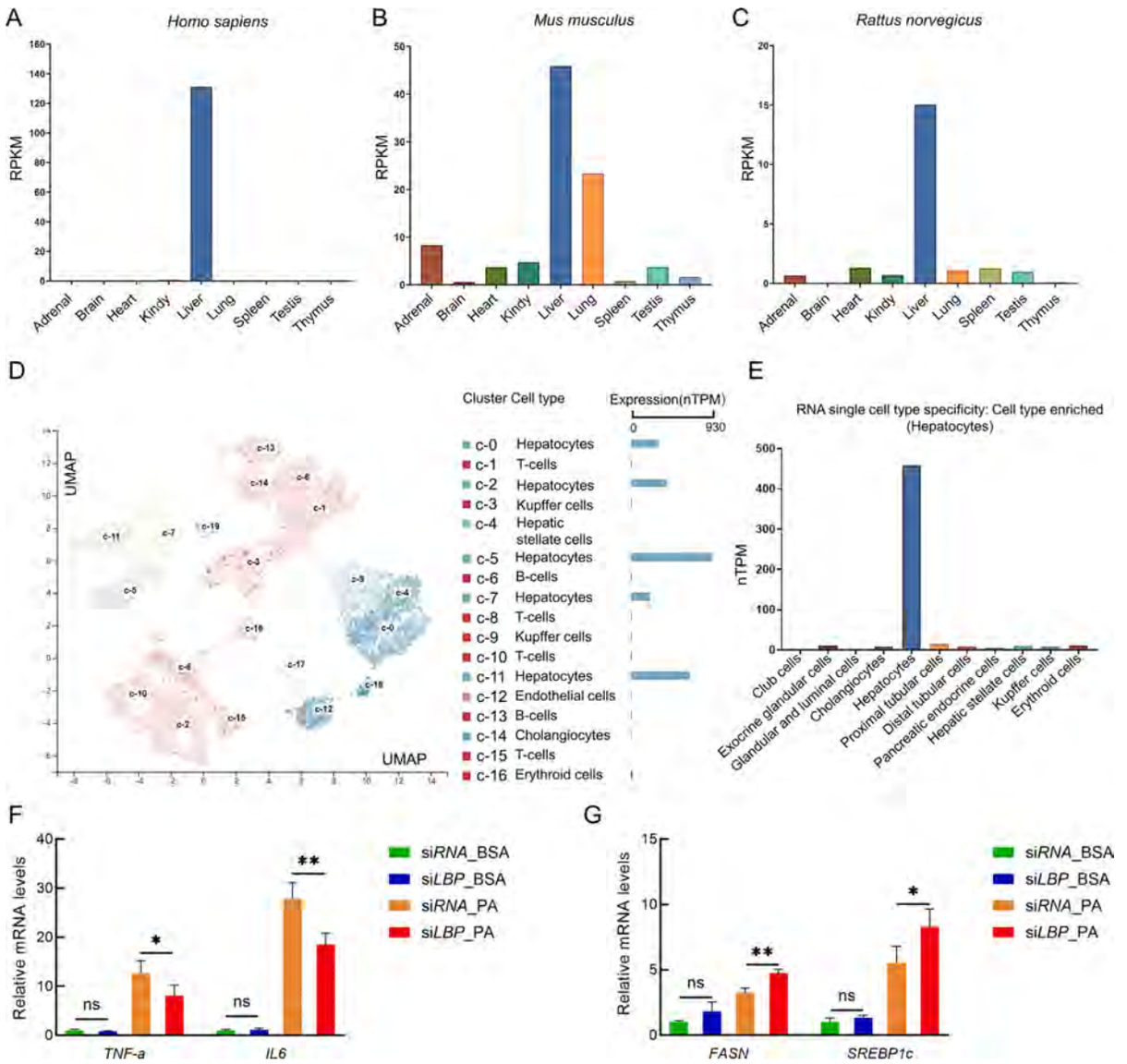

Figure 2 Hepatocyte-specific knockdown of *LBP* diminishes lipid accumulation

A–C: Tissue localization analysis of *LBP* in different tissues of *Homo sapiens* (A), *Mus musculus* (B), and *Rattus norvegicus* (C) using PRJEB443, PRJNA66167, and PRJNA238328 datasets, respectively, from NCBI public database (http://www.ncbi.nlm.nih.gov). D, E: Cellular localization analysis of *LBP* in different cell types in liver tissue (D) and all tissues (E) of humans using HPA public database (https://www.proteinatlas.org/). F, G: RT-qPCR analysis of mRNA levels of inflammation-related genes (F) and lipid deposition-related genes (G) of BRL-3A hepatocytes infected with indicated vectors, followed by stimulation with PA or BSA (n=3 independent experiments). One-way ANOVA of data was performed. ns: Not significant; *: P<0.05; **: P<0.01. All data are shown as mean±SD. PA: Palmitic acid, BSA: Bovine serum albumin, *TNF-α*: Tumor necrosis factor-α, *IL6*: Interleukin 6, *FASN*: Fatty acid synthase, *SREBP1c*: Sterol regulatory element binding protein 1c.

deteriorate lipid accumulation at the cellular level, corroborating observations noted in the animal models.

Transcriptome analysis reveals *LBP* deletion triggered lipid metabolic disorder in NAFLD rats

To further understand lipid deposition induced by *LBP* deletion, RNA-Seq of liver tissues from *LBP*$^{-/-}$ and WT rats fed a ND or HFD was conducted. In total, 168 and 3 871 significant DEGs (|$\log_2$(fold-change)|≥1.5 and P <0.05) were identified in the ND-fed *LBP*$^{-/-}$ rats and HFD-fed *LBP*$^{-/-}$ rats, respectively (Supplementary Figure S3A, B), consistent with our previous results showing more pronounced biological alterations in HFD-fed *LBP*-deficient rats compared to ND-fed *LBP*-deficient rats. The top 10 up-regulated and down-regulated genes in *LBP*$^{-/-}$_ND and *LBP*$^{-/-}$_HFD rats are shown in Supplementary Table S3 and S4, respectively. Functional analysis of these DEGs was conducted using DAVID (https://david.ncifcrf.gov/summary.jsp#) and Kyoto Encyclopedia of Genes and Genomes (KEGG) pathway analyses (https://www.genome.jp/kegg/). In the ND-fed rats, the DEGs induced by *LBP* deletion, including 101 up-regulated and 67 down-regulated genes, were markedly enriched in several biological processes, including "Endoplasmic reticulum membrane" and "Oxidation-reduction process" (Supplementary Figure S3A, C). For the HFD-fed rats, the DEGs induced by *LBP* deletion, including 2 402 up-regulated and 1 469 down-regulated genes, were enriched in various lipid metabolic processes, including "Oxidative acid metabolism", "Steroid metabolic process", and "Non-alcoholic fatty liver disease (NAFLD)" (Supplementary Figure S3B, D). Collectively, these results showed that *LBP* deletion

significantly interfered with the transcriptome profiles of HFD-fed rats, triggering abundant variation in gene expression and dysfunction in lipid metabolism, which may account for the excessive lipid deposition observed in the livers of HFD-induced NAFLD rats subjected to *LBP* knockout.

LBP deficiency contributes to H3K27 hyper-acetylation through the C/EBPβ TF

To examine the genome-wide cis-regulatory profiles of histone acetylome and transcriptome, ChIP-Seq analysis of H3K27ac, an important epigenetic marker of active enhancers, was applied to capture acetylated DNA regions and to determine alterations in acetylation levels induced by *LBP* deletion. Intriguingly, *LBP* deletion induced robust histone acetylome alteration in the HFD-fed rats compared to ND-fed rats. In total, 815 differential H3K27ac peaks ($|\log_2(\text{fold-change})|\geq 1$ and $P< 0.05$) were obtained in the livers of *LBP*$^{-/-}$_ND rats compared to WT_ND rats, including 279 hyper-acetylated and 536 hypo-acetylated peaks (Figure 3A, B). Furthermore, 2 116 differential H3K27ac peaks ($|\log_2(\text{fold-change})|\geq 1$ and $P<0.05$) were obtained in the livers of *LBP*$^{-/-}$_HFD rats compared to *LBP*$^{-/-}$_ND rats, including 891 hyper-acetylated and 1 225 hypo-acetylated peaks (Figure 3E, F). The top 10 ranked hyper- and hypo-acetylated peaks identified in the ND- and HFD-fed rats are shown in Supplementary Tables S5 and S6, respectively. Combined histone acetylome and transcriptome analysis revealed a consistent trend in gene expression and H3K27ac activity, suggesting a potential role of H3K27ac in regulating transcriptome gene expression.

To better understand the relationship between the acetylome and transcriptome, integrative acetylome H3K27ac ChIP-Seq and transcriptome RNA-Seq analysis was performed. Genome-wide "four-way" analysis identified significantly up-regulated peak-genes positively regulated by H3K27ac (PP peak-genes with up-regulated mRNA expression and positive H3K27ac density correlation) based on specific criteria ($|\log_2(\text{fold-change})|\geq 1.5$ and a Cor≥0.5). These findings were in accordance with expectations, with fewer PP peak-genes in *LBP*$^{-/-}$_ND rats (PP=48) than in *LBP*$^{-/-}$_HFD rats (PP=1 128) (Figure 3C, G). Regarding the PP peak-genes, loss of *LBP* in ND-fed rats primarily impacted fundamental biological processes, including the "Cytosol" (Figure 3D). In contrast, HFD-fed rats exhibited a pronounced over-representation of lipid deposition-related biological processes, including "Cholesterol metabolic process", "Fatty acid metabolic process", and "Lipid homeostasis" (Figure 3H), in accordance with the RNA-Seq results (Supplementary Figure S3C, D). These findings suggest that changes in H3K27ac activity may contribute to excessive lipid deposition in the liver of *LBP*$^{-/-}$ rats through changes in gene expression, prompting further investigation into the underlying mechanisms linking *LBP* knockout and the regulation of H3K27ac activity and lipid metabolism.

To identify core TFs, 15 PP peak-genes up-regulated in both *LBP*$^{-/-}$_ND and *LBP*$^{-/-}$_HFD rats were analyzed. Based on the novel method for core TF identification using integrative histone acetylome and transcriptome analysis, as detailed in Supplementary Figure S4, C/EBPβ was identified as a core TF. Notably, C/EBPβ was extensively modulated by the 15 intersecting PP peak-genes (Figure 3I; Supplementary Figure S5A) and emerged as the most relevant TF among 20 overlapping ones. Interestingly, previous studies have highlighted the role of C/EBPβ in epigenetics (Tamura et al., 2021) and lipid metabolism (Dörr et al., 2022). Both PPI network and GO enrichment analyses of the top 20 predicted TFs also emphasized the vital regulatory role of C/EBPβ (Figure 3J, Supplementary Figure S5B), especially regarding H3K27ac activity and lipid metabolism. To further validate the relationship between C/EBPβ and H3K27ac, H3K27ac peak Chr1:264178426-264189376 was identified as a core peak, indicative of genome-wide acetylation, with a shared differential peak induced by *LBP* deletion in both ND-fed and HFD-fed groups and markedly increased density in the C/EBPβ gene region (Supplementary Figure S5C, D). Further investigation confirmed the increase in C/EBPβ expression after *LBP* deletion and its positive correlation with H3K27ac in HFD-fed rats (Figure 3K–N).

The consistency of TF C/EBPβ and *LBP* gene interactions across species was analyzed following the workflow outlined in Supplementary Figure S4. Results indicated that *C/EBPβ* and *LBP* showed high homology among humans, rats, and mice, indicating high consistency in C/EBPβ-triggered transcriptional activation of *LBP* among these species (Figure 4A, B). The relationship between C/EBPβ and *LBP* was further confirmed by TF prediction based on *LBP* promoter sequences of the three species and *LBP* enhancer sequences of rats from the ChIP-Seq data. In total, 43 overlapping TFs were identified as targeting both *LBP* promoters and enhancers (Figure 4C). Among them, C/EBPβ emerged as the most relevant TF due to its extensive interactions with other TFs and related functions in epigeneticsand lipid metabolism (Figure 4D), consistent with previous results (Dörr et al., 2022; Tamura et al., 2021). Moreover, the Cistrome database (Zheng et al., 2019) also lists *C/EBPβ* as a potential transcriptional regulator of *LBP* in liver tissue (Figure 4E). Further RT-qPCR analysis validated the positive correlation between *C/EBPβ* and *LBP* (Figure 4F). Cumulatively, these findings indicate that the regulatory role C/EBPβ on *LBP* is highly consistent across humans, rats, and mice.

Based on the above results, *LBP* deletion appears to contribute to H3K27 hyper-acetylation in NAFLD rats through stimulation of C/EBPβ, providing further evidence for potential application in NAFLD cases in other species.

C/EBPβ significantly up-regulates *SCD* to promote liver lipid deposition

To investigate the potential mechanisms underlying altered H3K27ac-associated lipid accumulation, H3K27ac ChIP-Seq data analysis revealed increased genome-wide H3K27 acetylation within 3 kb of the TSS and transcript termination site (TES) in *LBP*$^{-/-}$_HFD rats, whereas a decline was observed in *LBP*$^{-/-}$_ND rats compared to their WT controls (Figure 5A, B). Hub targets of H3K27ac were subsequently searched using differential expression analysis of lipid metabolism-related genes based on the RNA-Seq data. Of note, *SCD* was identified as the most differentially expressed lipid metabolism-related gene (Figure 5C), in line with the ChIP-Seq results (Figure 5D), emphasizing the essential role of H3K27ac in the transcriptional activation of *SCD*. Further correlation and western blot analyses confirmed the positive correlation between *SCD* and H3K27ac, with enhanced protein levels after *LBP* knockout under HFD conditions (Figure 5E–G). Super-enhancer profiles of each group, derived from the H3K27ac ChIP-Seq data, revealed 456, 672, 837, and 892 super-enhancers in the livers of WT_ND, *LBP*$^{-/-}$

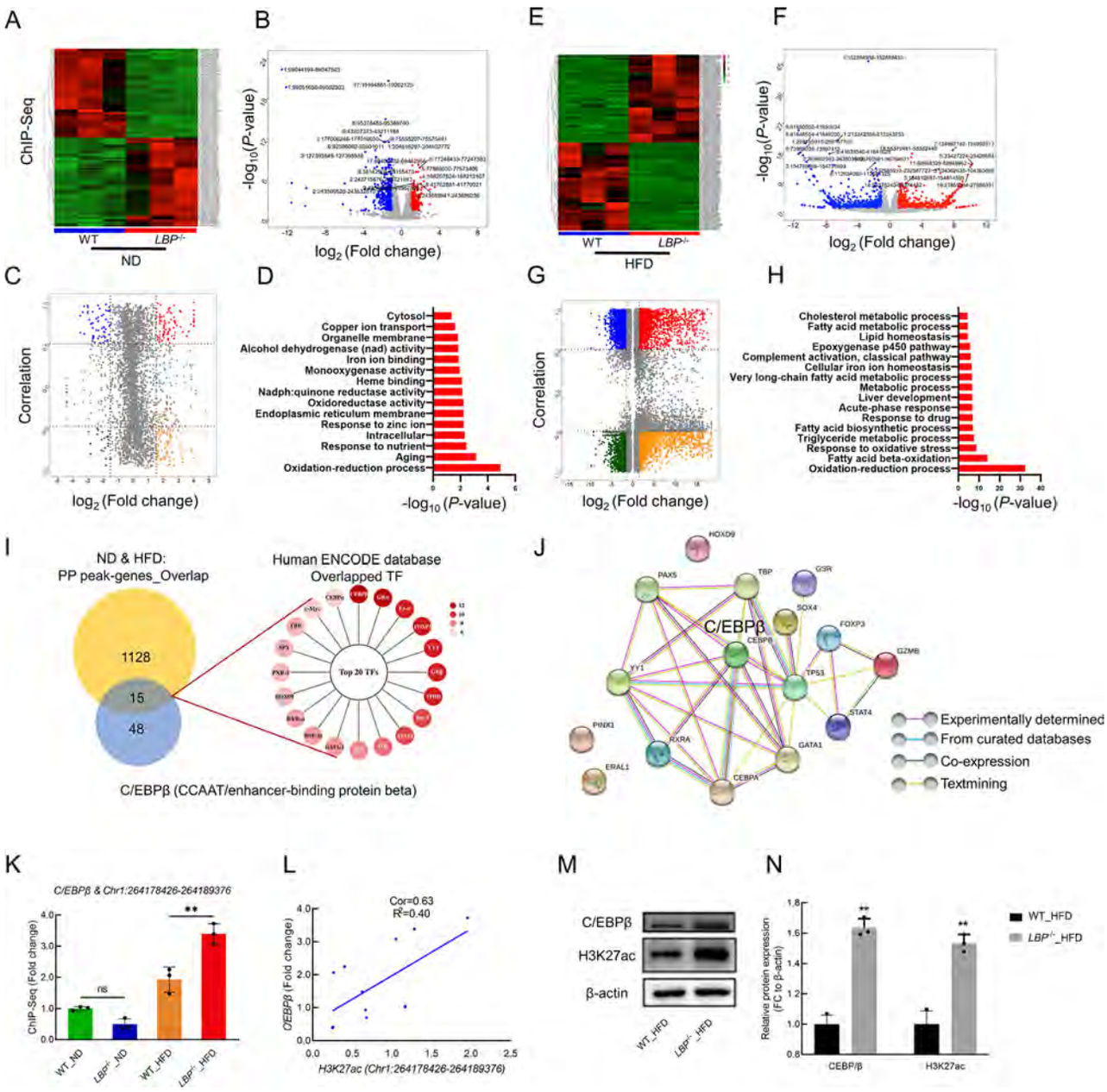

Figure 3 Integrative analysis of acetylome and transcriptome reveals upstream transcription factor C/EBPβ

A, B: Heatmap (A) and volcano plot (B) of differential H3K27ac regions between WT_ND and *LBP*$^{-/-}$_ND livers. Red and blue indicate up-regulation and down-regulation, respectively. C: Genome-wide "four-way" plot showing genes with |Cor (peak-gene correlation)|>0.5 and |$\log_2$(fold-change)|>1.5 generated by integrative H3K27ac ChIP-Seq and RNA-Seq analysis between WT_ND and *LBP*$^{-/-}$_ND rats. PP peak-genes with up-regulation and positive correlation are in red. D: Regulatory terms of PP peak-genes from ND_*LBP*$^{-/-}$ rats by DAVID (https://david-d.ncifcrf.gov/). E, F: Heatmap (E) and volcano plot (F) of differential H3K27ac regions between WT_ HFD and *LBP*$^{-/-}$_HFD livers. Red and blue indicate up-regulation and down-regulation, respectively. G: Genome-wide "four-way" plot showing genes with |Cor (peak-gene correlation)|>0.5 and |$\log_2$(fold-change)|>1.5 between WT and *LBP*$^{-/-}$ rats fed HFD, referred to in the legend of (C). H: Regulatory terms of PP peak-genes from *LBP*$^{-/-}$_ND rats by DAVID (https://david-d.ncifcrf.gov/). I: Venn diagram indicating overlapping PP peak-genes from livers of rats fed ND or HFD (left panel). Orange and blue circles indicate PP peak-genes from ND group (PP=48) and HFD group (PP=1 128), respectively. Right panel shows top 20 overlapping TFs identified in both ND and HFD groups using the Human ENCODE database (http://genome.ucsc.edu/ENCODE), identifying the most related TF (C/EBPβ). J: PPI diagram of most relevant TFs, using STRING v11.5 (https://cn.string-db.org/). K: Relative expression of *C/EBPβ&Chr1:264178426-264189376* from H3K27ac CHIP-Seq data in each group (*n*=3/group). L: Correlation between *C/EBPβ* expression level and H3K27ac peak (*Chr1:264178426-264189376*) density (Cor=0.63, R^2=0.4). M, N: Representative western blots (M) and quantification (N) of expression of C/EBPβ and H3K27ac protein levels in liver tissues from indicated rats (*n*=3/group). Student's *t*- test or one-way ANOVA was performed for data analysis as appropriate. ns: Not significant; **: *P*<0.01. Data are shown as mean±SD. ChIP-Seq: Chromatin immunoprecipitation coupled with high-throughput sequencing, RNA-Seq: Transcriptome high-throughput RNA sequencing, PP: up-regulated peak-genes positively regulated by H3K27ac ($\log_2$fold-change (ChIP≥0 & RNA≥0)), TF: Transcription factor, C/EBPβ: CCAAT/enhancer binding protein beta, H3K27ac: Histone H3 lysine 27 acetylation.

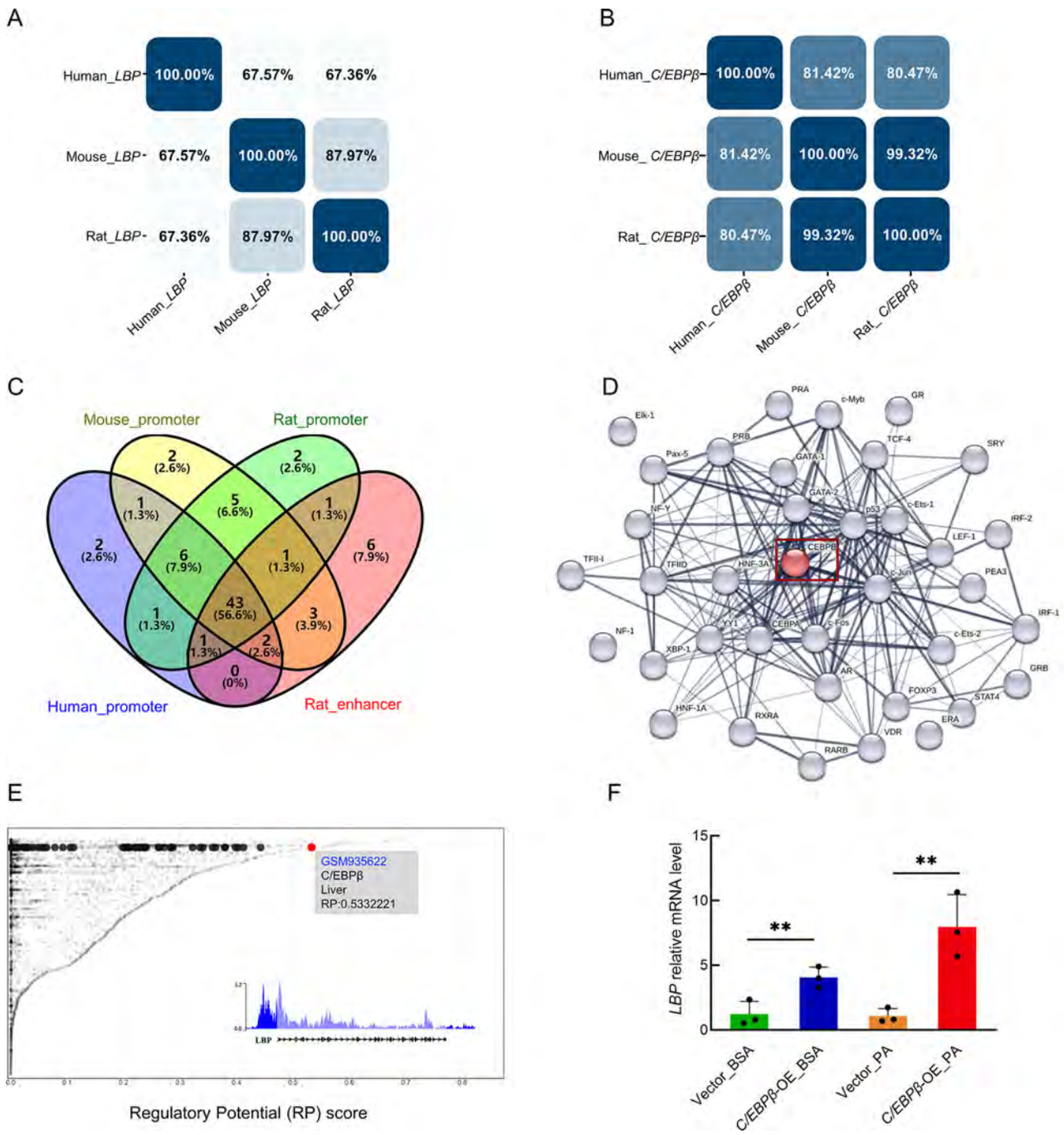

Figure 4 Regulatory process of C/EBPβ on *LBP* is highly consistent across humans, rats, and mice

A, B: Gene homology analysis of *LBP* (A) and *C/EBPβ* (B) among humans, rats, and mice using UniProt (https://www.uniprot.org/uniprot/). C: Venn diagram showing 43 overlapping TFs predicted by *LBP* promoter sequences of humans, mice, and rats from UCSC (http://www.genome.ucsc.edu/) and *LBP* enhancer sequences detected by H3K27ac ChIP-seq data. D: PPI network of top overlapping TFs in (C). E: Identification of C/EBPβ as a potential regulator of *LBP* gene in liver according to Cistrome database (accession number: GSM935622). All Cistrome data were carefully curated and processed with a streamlined analysis pipeline and evaluated with comprehensive quality control metrics. F: Relative mRNA levels of *LBP* in *C/EBPβ*-overexpressing BRL-3A cells and controls stimulated with PA or BSA (n=3/group). One-way ANOVA was performed for data analysis. **: P<0.01. Data are shown as mean±SD.

_ND, WT_HFD and *LBP*$^{-/-}$_HFD rats, respectively (Figure 6A, B, D, E). Interestingly, the *Chr1:264151393-264184386* super-enhancer, located proximal to the *SCD* gene region, exhibited pronounced activity in the *LBP*$^{-/-}$_HFD rats compared to the WT_HFD rats (Figure 6C, G). These findings suggest that H3K27 acetylation may facilitate the transcription and sustained expression of *SCD*, thus playing a vital role in the progression of HFD-induced NAFLD harboring *LBP* deletion.

Both RT-qPCR and Cistrome database analyses (Zheng et al., 2019) were performed, revealing a positive correlation between C/EBPβ and *SCD* (Figure 6F, H). C/EBPβ motifs and the top 10 potential C/EBPβ-binding sites in the SCD promoter region were identified using JASPAR (https://jaspar.genereg.net/) for subsequent regulatory functional analysis (Supplementary Figure S6). Of these, the top three binding sites were validated via a luciferase reporter assay, which

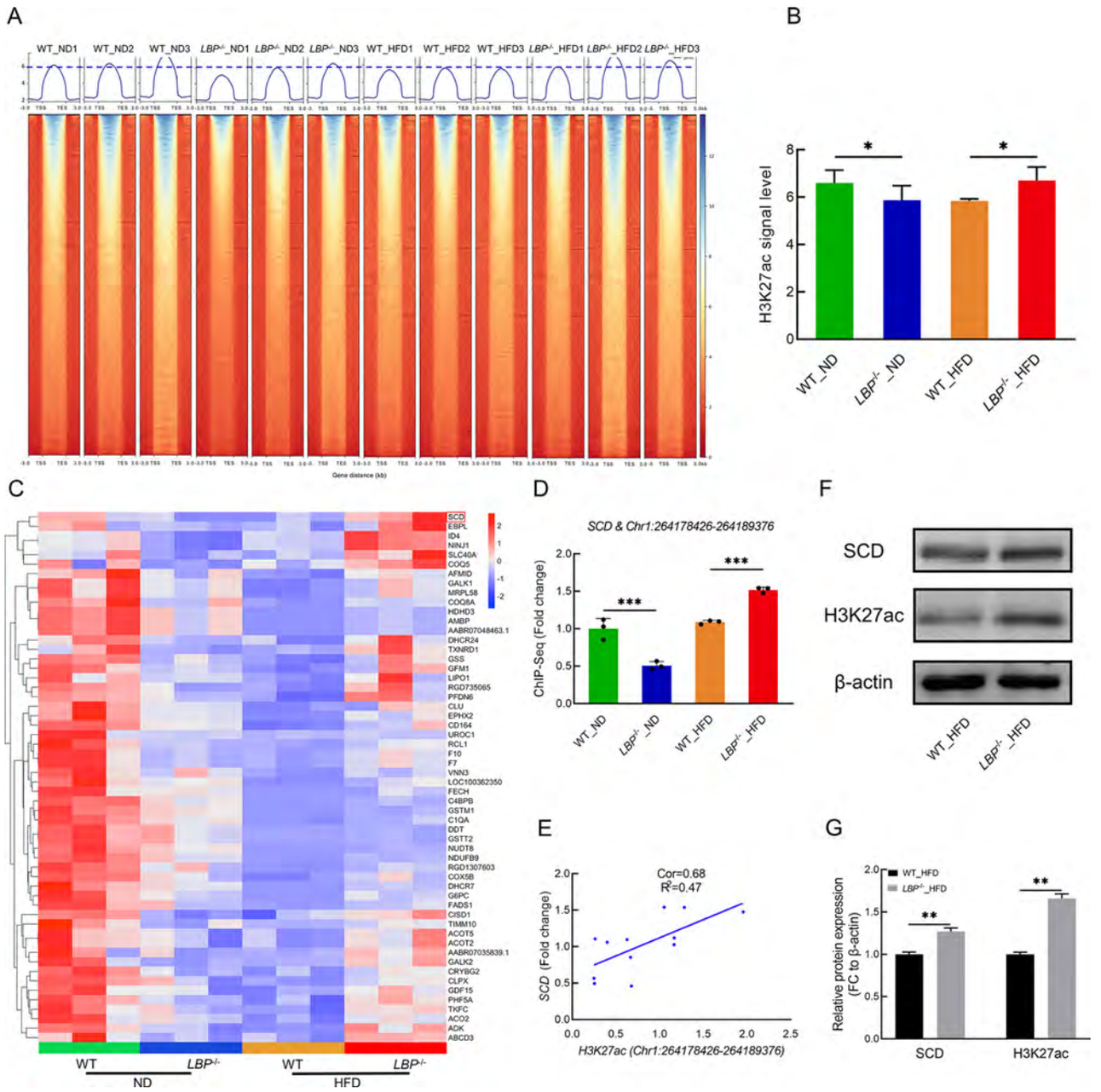

Figure 5 ***LBP*** **deficiency regulates expression of downstream lipid metabolism gene** ***SCD*** **through H3K27ac**

A: Heatmap showing H3K27ac signals at 3 kb near TSS and TES in the livers of WT_ND, *LBP*$^{-/-}$_ND, WT_HFD, and *LBP*$^{-/-}$_HFD rats (*n*=3/group). B: Quantification of H3K27ac signal level in each group, derived from ChIP-seq data shown in A (*n*=3/group). C: Heatmap of changes in mRNA levels of lipid metabolism-related genes in RNA-Seq data of liver from indicated groups (*n*=3/group). D: Relative expression of *SCD*&*Chr1:264178426-264189376* obtained by H3K27ac CHIP-Seq data in each group (*n*=3/group). E: Correlation between *SCD* expression level and H3K27ac peak (*Chr1:264178426-264189376*) density (Cor=0.68, R^2=0.47); F, G: Representative western blots (F) and quantification (G) of SCD and H3K27ac protein levels in liver tissues of WT_HFD and *LBP*$^{-/-}$_HFD rats (*n*=3/group). Student's *t*-test or one-way ANOVA was performed for data analysis. *: *P*<0.05; **: *P*<0.01; ***: *P*<0.001. Data are shown as mean±SD. TSS: Transcript start site, TES: Transcript termination site, *SCD*: Stearoyl-CoA desaturase.

signified that C/EBPβ substantially increased *SCD* activity, thereby highlighting the potential role of C/EBPβ in the transcriptional activation of *SCD* (Figure 6I, J). The DNA pull-down assay provided evidence of an interaction between *SCD* and C/EBPβ (Figure 6K), with the increase in the *SCD* mRNA level due to *C/EBPβ* overexpression further substantiated by RT-qPCR (Figure 6L). Together, these data suggest that C/EBPβ may promote the transcriptional activation of the lipid metabolism-related gene *SCD* during NAFLD in the context of *LBP* deficiency.

SCD accelerates excessive lipid deposition by inhibition of fatty acid oxidation (FAO)

To fully understand the functional metabolism of *SCD* in excessive lipid deposition, *SCD*-knockdown hepatocytes were established through siRNA transduction targeting the *SCD* gene, as confirmed by western blot and RT-qPCR (Supplementary Figure S7A, B). Results showed that *SCD* knockdown prominently decreased PA-induced lipid deposition but had little effect on BSA-treated hepatocytes (Supplementary Figure S7C). Consistently, hepatic TG was

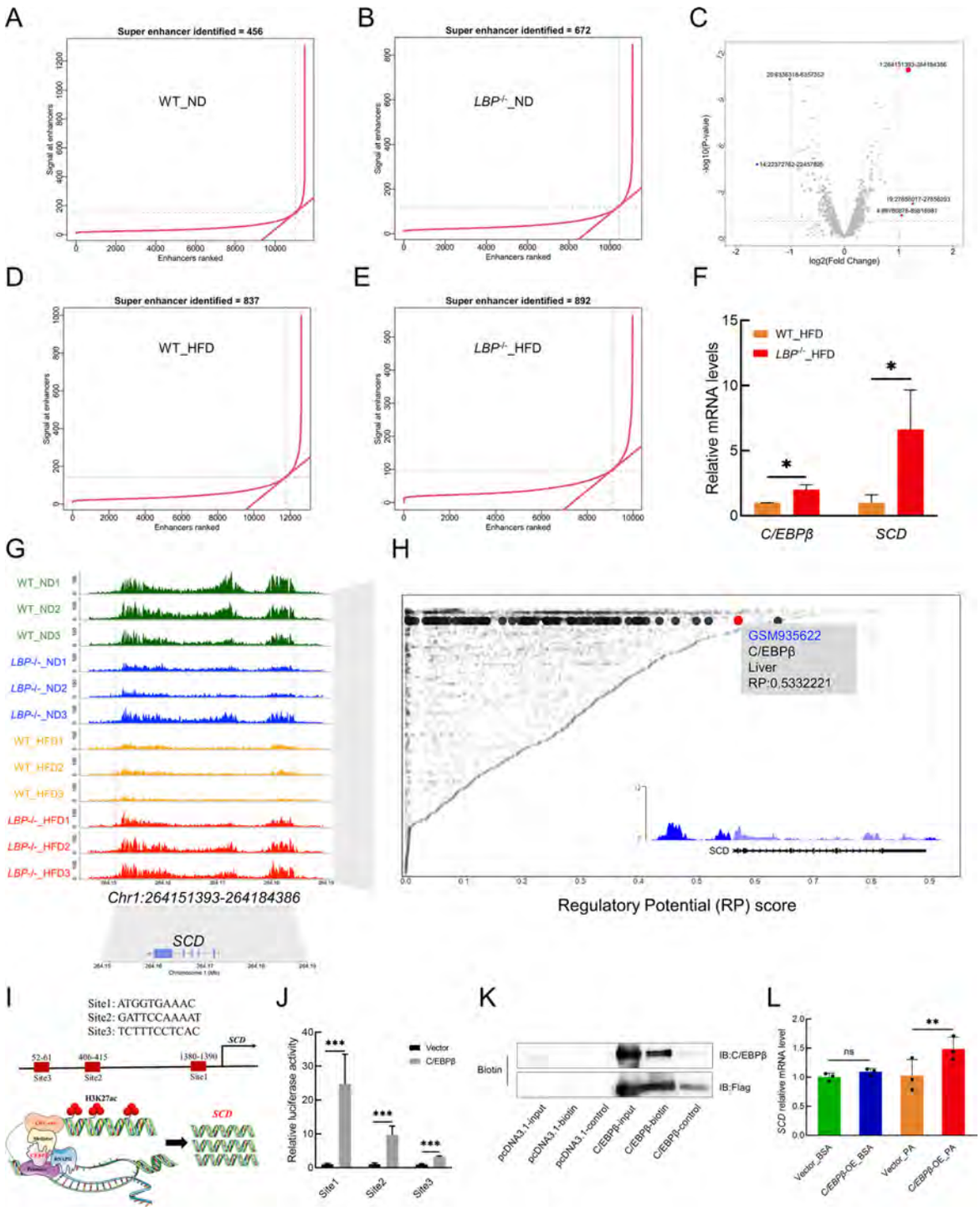

Figure 6 C/EBPβ facilitates expression of downstream lipid metabolism gene *SCD*

A, B: Enhancer regions of WT_ND (A) and *LBP*$^{-/-}$_ND (B) were plotted in increasing order based on their H3K27ac ChIP-seq signal. Enhancers above the curve inflection point were defined as super-enhancers. C: Volcano plots indicating significantly differential super-enhancers between WT_HFD and *LBP*$^{-/-}$_HFD samples. Red, blue, and gray dots indicate up-regulated, down-regulated, and unchanged H3K27ac peaks, respectively. D, E: Enhancer regions of WT_HFD (D) and *LBP*$^{-/-}$_HFD (E) were plotted in increasing order based on their H3K27ac ChIP-seq signal. Enhancers above the curve inflection point were defined as super-enhancers. F: Relative mRNA levels of *C/EBPβ* and *SCD* in HFD-fed *LBP*$^{-/-}$ and WT rats (*n*=3/group). G: Genome browser representation showing activity of *Chr1:264151393-264184386* super-enhancer, which tracks at the *SCD* locus in indicated individuals (*n*=3/group). H: Identification of C/EBPβ as a potential regulator of *SCD* gene in liver according to the Cistrome database (accession number: GSM935622). I: Schematic of three potential binding sites for C/EBPβ in *SCD* promoter region (upper panel) and model of enhanced *SCD* expression induced by C/EBPβ (lower panel). J: Relative activities of luciferase vectors in BRL-3A hepatocytes transfected with C/EBPβ and vector at predicted C/EBPβ-binding sites (site 1, site 2, site 3) in *SCD* promoter region (*n*=3/group). K: DNA pull-down assay showing interaction between C/EBPβ-binding site 1 in *SCD* promoter region and exogenous C/EBPβ. L: Relative mRNA levels of *SCD* in *C/EBPβ*-overexpressing BRL-3A cells and controls stimulated with PA or BSA (*n*=3/group). Student's *t*-test or one-way ANOVA was performed for data analysis. ns: Not significant; *: P<0.05; **: P<0.01; ***: P<0.001. Data are shown as mean±SD.

also significantly decreased following *SCD* knockdown and PA exposure compared to the controls, while the BSA group demonstrated no significant changes (Supplementary Figure S7D). These data suggest that *SCD* is essential for the progression of excessive lipid deposition in PA-induced hepatocytes. We further investigated the critical role of *SCD* in the progression of NAFLD deterioration induced by *LBP* deficiency *in vitro* and *in vivo*. Metabolomic analysis revealed elevated fatty acid content in *LBP*$^{-/-}$_HFD livers compared to WT_HFD livers (Supplementary Figure S8), as well as positive correlations between *SCD* expression and NAFLD parameters, including serum TG, TC, ALT, and AST levels, in *LBP*$^{-/-}$ rats (Supplementary Figure S9). In line with the *in vivo* observations, SCD inhibition in hepatocytes also significantly reversed the accelerated lipid accumulation induced by si*LBP* (Figure 7A; Supplementary Figure S10), further confirming the critical role of *SCD* in *LBP* deficiency- induced accelerated hepatocyte lipid deposition. Given the potential effects of *SCD* on accelerating lipid deposition through regulation of FAO (Kim et al., 2011), the mRNA expression levels of key genes positively associated with FAO activity (Supplementary Table S7) were measured in the livers of *LBP*-deficient HFD-induced NAFLD mice, confirming the role of *SCD* in excessive lipid deposition through dysfunctional FAO. Interestingly, *LBP* depletion-triggered overexpression of *SCD* robustly impaired the mRNA expression levels of FAO-related genes compared to the controls (Figure 7B–I). Together, these results suggest that *SCD* may contribute to excessive lipid deposition in the liver by inhibiting FAO in NAFLD harboring *LBP* deficiency.

DISCUSSION

In the present study, the potential epigenetic

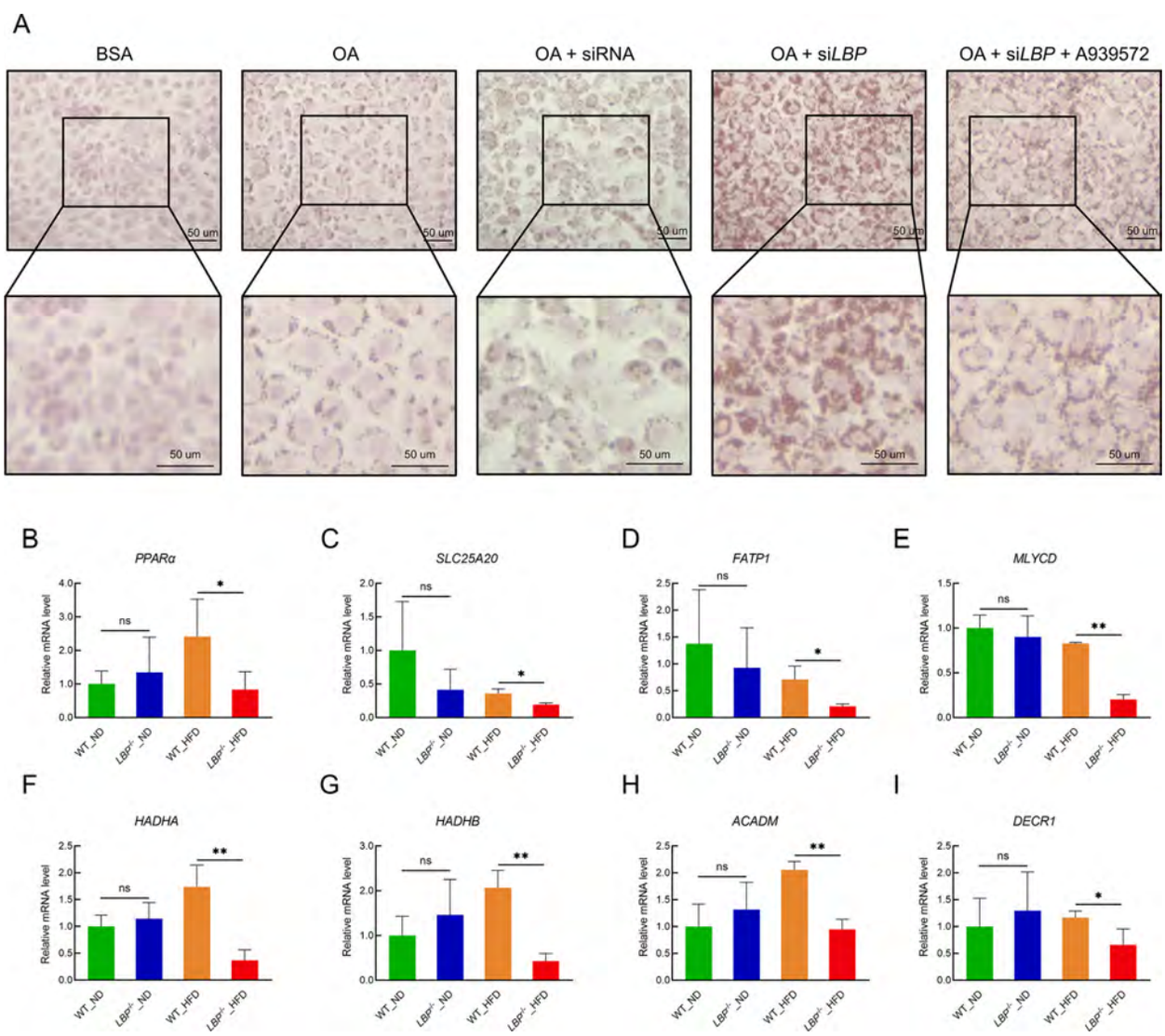

Figure 7 Regulatory mechanism of *SCD* aggravating lipid metabolic disorder of HFD-induced NAFLD with *LBP* deficiency

A: Images of Oil-red O staining of BRL-3A hepatocytes in indicated groups (n=3/group). Scale bar: 50 μm. B–I: Relative mRNA expression levels of FAO-related genes *PPARα* (B), *SLC25A20* (C), *FATP1* (D), *MLYCD* (E), *HADHA* (F), *HADHB* (G), *ACADM* (H), and *DECR1* (I) in liver tissues from WT_ND, *LBP*$^{-/-}$_ND, WT_HFD, and *LBP*$^{-/-}$_HFD rats (n=3/group). One-way ANOVA was performed for data analysis. ns: Not significant; *: P<0.05; **: P<0.01. Data are shown as mean±*SD*. *PPARα*: Peroxisome proliferator-activated receptor α, *SLC25A20*: Solute carrier family 25 member 20, *FATP1*: Fatty acid transport protein 1, *MLYCD*: Malonyl-CoA decarboxylase, *HADHA*: Hydroxyacyl-CoA dehydrogenase trifunctional multienzyme complex subunit alpha, *HADHB* : Hydroxyacyl-CoA dehydrogenase trifunctional multienzyme complex subunit beta, *ACADM* : Acyl-CoA dehydrogenase medium chain, *DECR1*: Mitochondrial 2,4-dienoyl-CoA reductase 1.

pathomechanisms of *LBP* deficiency as a potent contributor to NAFLD exacerbation were investigated. Results indicated that *LBP* knockout reduced inflammation but exacerbated HFD-induced NAFLD development through excessive lipid deposition. Through integrative histone acetylome H3K27ac ChIP-Seq and transcriptome RNA-Seq analysis, several related TFs and genes were identified in NAFLD livers harboring *LBP* deficiency. Among these, C/EBPβ was identified as an essential TF for dysregulated H3K27ac and *SCD*, transcriptionally activated by C/EBPβ, was identified as a hub gene and key mediator of NAFLD progression in *LBP*$^{-/-}$ rats. Taken together, this study provides insights into the epigenetic mechanisms underpinning HFD-induced NAFLD pathogenesis in the context of *LBP* deficiency, identifying potential TFs and key genes as potential candidate therapeutic targets.

LBP, recognized for its crucial role in inflammatory response regulation (Meng et al., 2021), has also been implicated in nutritional metabolic diseases (Nien et al., 2018; Sun et al., 2010). However, the precise mechanism by which *LBP* functions in NAFLD remains unclear, particularly in terms of epigenetic processes. In the current study, an *LBP*-knockout NAFLD model was utilized, replicating outcomes observed in clinical cases of *LBP* mutation. Based upon this model, *LBP* deficiency was identified as a potent contributor to NAFLD exacerbation from an epigenetics perspective. Results also revealed prominent liver specificity of *LBP* and distinct dysfunction in lipid metabolism-related processes in NAFLD with *LBP* knockout, consistent with the potential induction role of *LBP*$^{-/-}$ in liver lipid metabolism disorders. To further explore the epigenetic mechanisms and pathogenesis underlying the effects of *LBP* on NAFLD, we constructed H3K27ac alteration profiles and transcriptome maps, revealing widespread NAFLD-associated histone acetylome and transcriptome variation induced by *LBP* depletion. These observations align with the notion that dysregulation of H3K27ac is instrumental in modulating the development of fatty liver diseases by facilitating gene transcriptional activation (Li et al., 2021; Sun et al., 2015; Zhu et al., 2021).

Moreover, mediation of TF binding motifs is viewed as a critical mechanism of histone acetylome-induced gene transcriptional activation (Hsieh et al., 2022; Lambert et al., 2018; Marzi et al., 2018), highlighting the importance of TFs as potential therapeutic targets for NAFLD (Liang et al., 2019; Zhao et al., 2022b). Nevertheless, methods for the systematic prediction of core TFs are still lacking. Here, a model for the systematic screening of core TFs was developed using integrative histone acetylome and transcriptome analysis. Results revealed the potential significance of C/EBPβ, recognized as a key early regulator of adipogenesis (Feng et al., 2016; Moseti et al., 2016; Xi et al., 2016), in the progression of H3K27 hyper-acetylation induced by *LBP* deficiency in HFD-fed rats. Previous studies have identified C/EBPβ as a critical factor in the promoter and enhancer regions of genes (Takagi et al., 2022) and in the genome-wide increase of H3K27ac and various genes (Tamura et al., 2021), consistent with our findings of C/EBPβ-induced H3K27 hyper-acetylation and enhanced *SCD* gene expression. These results broaden our understanding of the biological functions of C/EBPβ in NAFLD and support C/EBPβ as a key player in the pathogenesis of NAFLD under *LBP* deficiency.

Our results also indicated that *SCD* may serve as a downstream effector of H3K27ac and C/EBPβ. Deficiency of *LBP* resulted in pronounced H3K27 hyper-acetylation, which facilitated the binding of C/EBPβ to the promoter region, leading to the activation of *SCD*. This gene, a vital marker of lipid metabolism, is frequently associated with the acceleration of fatty liver disorder progression due to its role in lipid deposition (Klepp et al., 2022; Zhang et al., 2020). Emerging evidence has suggested that *SCD* plays a potential role in triggering lipid accumulation through FAO suppression (Dobrzyn et al., 2004; Kim et al., 2011; Ntambi et al., 2002), as confirmed by the decreased expression of various FAO-related genes in our study. Differential super-enhancers with increased intensity in the *SCD* gene region were observed, consistent with H3K27ac ChIP-Seq data showing marked H3K27ac occupancy post-*LBP* deletion and HFD feeding, correlated with elevated mRNA expression. Collectively, these findings emphasize the key roles of C/EBPβ in *SCD* expression elevation and FAO inhibition in the current NAFLD model with *LBP* depletion. However, comprehensive research is needed to fully delineate the downstream network contributing to the hepatic roles of C/EBPβ.

Based on dysregulated acetylation and peak-genes, as well as the enriched TF binding motif of C/EBPβ and *SCD* gene, we proposed a potential epigenetic regulation mechanism in HFD-induced NAFLD livers harboring *LBP* deletion (Figure 8). In this model, *LBP* deficiency may trigger C/EBPβ, driving genome-wide histone hyper-acetylation and transcriptional activation of *SCD* through the binding motif of C/EBPβ, resulting in FAO inhibition in hepatocytes and exacerbation of HFD-induced NAFLD pathogenesis.

To the best of our knowledge, this is the first study to present genome-wide profiling of acetylation and transcription signals underlying the pathogenesis of NAFLD related to *LBP* deficiency. However, several study limitations should be mentioned. Firstly, the applicability of the results to other diet-induced NAFLD models, such as Western-style diet (WSD)-induced or methionine- and choline-deficient diet (MCD)-induced NAFLD models, is unknown. Notably, Jin et al. (2017) reported that loss of *LBP* can attenuate the development of WSD-induced NAFLD, which is inconsistent with our results. It is well established that the clinical pathogenesis and characteristics of NAFLD are highly heterogeneous (Yang et al., 2021). Thus, different diets may trigger different hepatic pathological features, mimicking different clinical states of NAFLD, which may explain the different influences of *LBP* deficiency on NAFLD. Additionally, although our sample size met the requirements for statistical analysis and was sufficient for determining the findings described above, future studies with larger sample sizes are essential for mitigating potential confounding factors and reinforcing these findings. Further in-depth experimental validation and molecular mechanism elucidation are required, which will be the focus of our future work.

In conclusion, while certain questions remain to be elucidated, these findings provide valuable insights into the epigenetic pathomechanisms underlying HFD-induced NAFLD with *LBP* depletion. Our results revealed robust alterations in histone acetylome H3K27ac and transcriptome as well as marked dysfunction in lipid metabolism-related biological processes induced by *LBP* knockout. Furthermore, based on integrative H3K27ac ChIP-seq and RNA-seq data analysis, C/EBPβ was identified as a core TF and driver of pathogenesis. Additionally, downstream effector *SCD*, a lipid

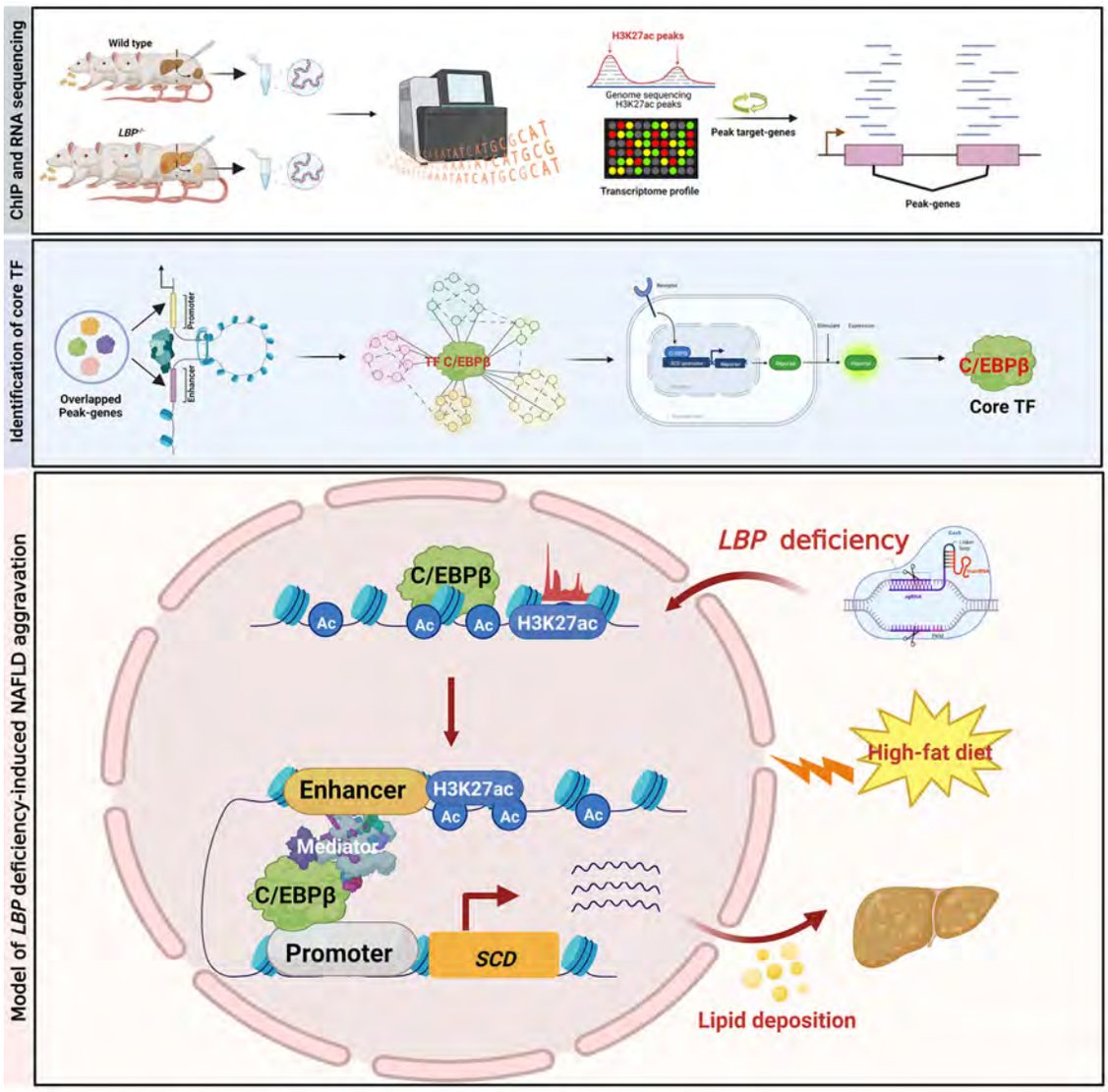

Figure 8 Proposed model of *LBP* deficiency exacerbating HFD-induced NAFLD pathogenesis

In this epigenetic mechanism-based model, C/EBPβ was identified as a pivotal TF and contributor to the progression of HFD-induced NAFLD with *LBP* deletion based on integrative H3K27ac ChIP-Seq and RNA-Seq analysis. Thus, *LBP* deficiency may trigger C/EBPβ to drive genome-wide histone H3 hyper- acetylation and activate transcriptional expression of downstream effector *SCD* to exacerbate NAFLD pathogenesis. Graph was created with BioRender software (https://biorender.com/)

metabolism gene with elevated super-enhancer activity in the gene region, was confirmed to accelerate excessive liver lipid deposition by inhibiting FAO. C/EBPβ and *SCD* were screened as core drivers of the pathogenesis of HFD-induced NAFLD with *LBP* depletion, and thus may serve as effective therapeutic targets.

DATA AVAILABILITY

The raw data reported in this paper were deposited in the National Center for Biotechnology Information Sequence Read Archive (NCBI SRA: PRJNA1044849), National Genomics Data Center (GSA: PRJCA017968 and PRJCA002667), and Science Data Bank (DOI:10.57760/sciencedb.09322). All data that support the findings of this study are available from the corresponding authors upon request.

COMPETING INTERESTS

The authors declare they have no competing interests.

AUTHOR'S CONTRIBUTATIONS

H.S.F. and F.H. designed the experiments. Y.L.Z., L.L.M., and J.H.M. performed the experiments and completed the manuscript. X.Y., Y.S.T., M.X., and S.W.C. performed the cell experiments. X.R.Y. and X.Y.L. preformed animal experiments. Y.W. and M.Z.Z. analyzed the H3K27ac ChIP-Seq and RNA-Seq data. J.P. and X.J.L. conducted the core transcription factor prediction. J.Z.H. conducted the integrative ChIP-Seq and RNA-Seq analyses. Z.C.S., C.W., K.Z.Z., and Q.Q.D. analyzed most of the experimental data. All authors read and approved the final version of the manuscript.

ACKNOWLEDGMENTS

We are grateful to colleagues from the Laboratory Animal Research Center, Anhui Medical University, for animal husbandry and sample collection, and the College of Animal Science and Technology, Jiangxi Agricultural University, for the ChIP experiments.

REFERENCES

Abuín JM, Pichel JC, Pena TF, et al. 2015. BigBWA: approaching the burrows-wheeler aligner to big data technologies. *Bioinformatics*, **31**(24): 4003−4005.

Becares N, Gage MC, Voisin M, et al. 2019. Impaired LXRα phosphorylation attenuates progression of fatty liver disease. *Cell Reports*, **26**(4): 984−995.e6.

Brunt EM, Kleiner DE, Wilson LA, et al. 2011. Nonalcoholic fatty liver disease (NAFLD) activity score and the histopathologic diagnosis in NAFLD: distinct clinicopathologic meanings. *Hepatology*, **53**(3): 810−820.

Dobin A, Davis CA, Schlesinger F, et al. 2013. STAR: ultrafast universal RNA-seq aligner. *Bioinformatics*, **29**(1): 15−21.

Dobrzyn P, Dobrzyn A, Miyazaki M, et al. 2004. Stearoyl-CoA desaturase 1 deficiency increases fatty acid oxidation by activating AMP-activated protein kinase in liver. *Proceedings of the National Academy of Sciences of the United States of America*, **101**(17): 6409−6414.

Dörr D, Obermayer B, Weiner JM, et al. 2022. C/EBPβ regulates lipid metabolism and *Pparg* isoform 2 expression in alveolar macrophages. *Science Immunology*, **7**(75): eabj0140.

Feinberg AP. 2007. Phenotypic plasticity and the epigenetics of human disease. *Nature*, **447**(7143): 433−440.

Feng S, Reuss L, Wang Y. 2016. Potential of natural products in the inhibition of adipogenesis through regulation of PPARγ expression and/or its transcriptional activity. *Molecules*, **21**(10): 1278.

Friedman SL, Neuschwander-Tetri BA, Rinella M, et al. 2018. Mechanisms of NAFLD development and therapeutic strategies. *Nature Medicine*, **24**(7): 908−922.

Hsieh WC, Sutter BM, Ruess H, et al. 2022. Glucose starvation induces a switch in the histone acetylome for activation of gluconeogenic and fat metabolism genes. *Molecular Cell*, **82**(1): 60−74.e5.

Hu MJ, Long M, Dai RJ. 2022. Acetylation of H3K27 activated lncRNA NEAT1 and promoted hepatic lipid accumulation in non-alcoholic fatty liver disease via regulating miR-212-5p/GRIA3. *Molecular and Cellular Biochemistry*, **477**(1): 191−203.

Jin CJ, Engstler AJ, Ziegenhardt D, et al. 2017. Loss of lipopolysaccharide-binding protein attenuates the development of diet-induced non-alcoholic fatty liver disease in mice. *Journal of Gastroenterology and Hepatology*, **32**(3): 708−715.

Kim E, Lee JH, Ntambi JM, et al. 2011. Inhibition of stearoyl-CoA desaturase1 activates AMPK and exhibits beneficial lipid metabolic effects *in vitro*. *European Journal of Pharmacology*, **672**(1–3): 38–44.

Klepp TD, Sloan ME, Soundararajan S, et al. 2022. Elevated stearoyl-CoA desaturase 1 activity is associated with alcohol-associated liver disease. *Alcohol*, **102**: 51−57.

Lambert SA, Jolma A, Campitelli LF, et al. 2018. The human transcription factors. *Cell*, **172**(4): 650−665.

Li H, Handsaker B, Wysoker A, et al. 2009. The sequence alignment/map format and SAMtools. *Bioinformatics*, **25**(16): 2078−2079.

Li XZ, Yuan BC, Lu M, et al. 2021. The methyltransferase METTL3 negatively regulates nonalcoholic steatohepatitis (NASH) progression. *Nature Communications*, **12**(1): 7213.

Liang N, Damdimopoulos A, Goñi S, et al. 2019. Hepatocyte-specific loss of GPS2 in mice reduces non-alcoholic steatohepatitis via activation of PPARα. *Nature Communications*, **10**(1): 1684.

Liu Y, Jiang L, Sun CX, et al. 2018. Insulin/snail1 axis ameliorates fatty liver disease by epigenetically suppressing lipogenesis. *Nature Communications*, **9**(1): 2751.

Love MI, Huber W, Anders S. 2014. Moderated estimation of Fold change and dispersion for RNA-seq data with DESeq2. *Genome Biology*, **15**(12): 550.

Marzi SJ, Leung SK, Ribarska T, et al. 2018. A histone acetylome-wide association study of Alzheimer's disease identifies disease-associated H3K27ac differences in the entorhinal cortex. *Nature Neuroscience*, **21**(11): 1618−1627.

Meng LL, Song ZC, Liu AD, et al. 2021. Effects of lipopolysaccharide-binding protein (LBP) single nucleotide polymorphism (SNP) in infections, inflammatory diseases, metabolic disorders and cancers. *Frontiers in Immunology*, **12**: 681810.

Moreno-Navarrete JM, Escoté X, Ortega F, et al. 2015. Lipopolysaccharide binding protein is an adipokine involved in the resilience of the mouse adipocyte to inflammation. *Diabetologia*, **58**(10): 2424−2434.

Moseti D, Regassa A, Kim WK. 2016. Molecular regulation of adipogenesis and potential anti-adipogenic bioactive molecules. *International Journal of Molecular Sciences*, **17**(1): 124.

Nien HC, Sheu JC, Chi YC, et al. 2018. One-year weight management lowers lipopolysaccharide-binding protein and its implication in metainflammation and liver fibrosis. *Plos One*, **13**(11): e0207882.

Ntambi JM, Miyazaki M, Stoehr JP, et al. 2002. Loss of stearoyl-CoA desaturase-1 function protects mice against adiposity. *Proceedings of the National Academy of Sciences of the United States of America*, **99**(17): 11482−11486.

Ospelt C. 2022. A brief history of epigenetics. *Immunology Letters*, **249**: 1−4.

Pfalzgraff A, Weindl G. 2019. Intracellular lipopolysaccharide sensing as a potential therapeutic target for sepsis. *Trends in Pharmacological Sciences*, **40**(3): 187−197.

Quinlan AR, Hall IM. 2010. BEDTools: a flexible suite of utilities for comparing genomic features. *Bioinformatics*, **26**(6): 841−842.

Rada-Iglesias A, Bajpai R, Swigut T, et al. 2011. A unique chromatin signature uncovers early developmental enhancers in humans. *Nature*, **470**(7333): 279−283.

Samuel VT, Shulman GI. 2018. Nonalcoholic fatty liver disease as a nexus of metabolic and hepatic diseases. *Cell Metabolism*, **27**(1): 22−41.

Sewe SO, Silva G, Sicat P, et al. 2022. Trimming and validation of illumina short reads using trimmomatic, trinity assembly, and assessment of RNA-seq data. *In*: Edwards D. Plant Bioinformatics: Methods and Protocols. New York: Springer, 211–232.

Smith E, Shilatifard A. 2014. Enhancer biology and enhanceropathies. *Nature Structural & Molecular Biology*, **21**(3): 210−219.

Soneson C, Love MI, Robinson MD. 2015. Differential analyses for RNA-seq: transcript-level estimates improve gene-level inferences. *F1000Research*, **4**: 1521.

Song ZC, Meng LL, He ZX, et al. 2021. LBP protects hepatocyte mitochondrial function via the PPAR-CYP4A2 signaling pathway in a rat sepsis model. *Shock*, **56**(6): 1066−1079.

Sun C, Fan JG, Qiao L. 2015. Potential epigenetic mechanism in non-alcoholic fatty liver disease. *International Journal of Molecular Sciences*, **16**(3): 5161−5179.

Sun L, Yu ZJ, Ye XW, et al. 2010. A marker of endotoxemia is associated with obesity and related metabolic disorders in apparently healthy Chinese. *Diabetes Care*, **33**(9): 1925−1932.

Szklarczyk D, Morris JH, Cook H, et al. 2017. The STRING database in 2017: quality-controlled protein-protein association networks, made broadly accessible. *Nucleic Acids Research*, **45**(D1): D362−D368.

Takagi H, Tamura I, Fujimura T, et al. 2022. Transcriptional coactivator PGC-1α contributes to decidualization by forming a histone-modifying complex with C/EBPβ and p300. *Journal of Biological Chemistry*, **298**(5): 101874.

Takahashi JS, Kumar V, Nakashe P, et al. 2015. ChIP-seq and RNA-seq methods to study circadian control of transcription in mammals. *Methods in Enzymology*, **551**: 285−321.

Takeuchi F, Yanai K, Inomata H, et al. 2007. Search of type 2 diabetes susceptibility gene on chromosome 20q. *Biochemical and Biophysical Research Communications*, **357**(4): 1100−1106.

Tamura I, Maekawa R, Jozaki K, et al. 2021. Transcription factor C/EBPβ induces genome-wide H3K27ac and upregulates gene expression during

decidualization of human endometrial stromal cells. *Molecular and Cellular Endocrinology*, **520**: 111085.
Villar D, Berthelot C, Aldridge S, et al. 2015. Enhancer evolution across 20 mammalian species. *Cell*, **160**(3): 554−566.
Whyte WA, Orlando DA, Hnisz D, et al. 2013. Master transcription factors and mediator establish super-enhancers at key cell identity genes. *Cell*, **153**(2): 307−319.
Xi Y, Shen WJ, Ma LL, et al. 2016. HMGA2 promotes adipogenesis by activating C/EBPβ-mediated expression of PPARγ. *Biochemical and Biophysical Research Communications*, **472**(4): 617−623.
Yang X, Sun DT, Xiang H, et al. 2021. Hepatocyte SH3RF2 deficiency is a key aggravator for NAFLD. *Hepatology*, **74**(3): 1319−1338.
Younossi Z, Tacke F, Arrese M, et al. 2019. Global perspectives on nonalcoholic fatty liver disease and nonalcoholic steatohepatitis. *Hepatology*, **69**(6): 2672−2682.
Youssefian L, Vahidnezhad H, Saeidian AH, et al. 2019. Inherited non-alcoholic fatty liver disease and dyslipidemia due to monoallelic *ABHD5* mutations. *Journal of Hepatology*, **71**(2): 366−370.
Yu Y, Cai JJ, She ZG, et al. 2019. Insights into the epidemiology, pathogenesis, and therapeutics of nonalcoholic fatty liver diseases. *Advanced Science*, **6**(4): 1801585.
Zhang N, Wang YL, Zhang JL, et al. 2020. N-glycosylation of CREBH improves lipid metabolism and attenuates lipotoxicity in NAFLD by modulating PPARα and SCD-1. *The FASEB Journal*, **34**(11): 15338−15363.
Zhang Y, Liu T, Meyer CA, et al. 2008. Model-based analysis of ChIP-seq (MACS). *Genome Biology*, **9**(9): R137.
Zhao N, Zhang XX, Ding JJ, et al. 2022a. *SEMA7A*^{R148W} mutation promotes lipid accumulation and NAFLD progression via increased localization on the hepatocyte surface. *JCI insight*, **7**(15): e154113.
Zhao S, Zhang XR, Li HT. 2018. Beyond histone acetylation—writing and erasing histone acylations. *Current Opinion in Structural Biology*, **53**: 169−177.
Zhao YC, Gao LC, Jiang CL, et al. 2022b. The transcription factor zinc fingers and homeoboxes 2 alleviates NASH by transcriptional activation of phosphatase and tensin homolog. *Hepatology*, **75**(4): 939−954.
Zheng RB, Wan CX, Mei SL, et al. 2019. Cistrome data browser: expanded datasets and new tools for gene regulatory analysis. *Nucleic Acids Research*, **47**(D1): D729−D735.
Zhou Z, Xu MJ, Gao B. 2016. Hepatocytes: a key cell type for innate immunity. *Cellular & Molecular Immunology*, **13**(3): 301−315.
Zhu YL, Zeng QJ, Li F, et al. 2021. Dysregulated H3K27 acetylation is implicated in fatty liver hemorrhagic syndrome in chickens. *Frontiers in Genetics*, **11**: 574167.